# Whole-chromosome duplications drive antimicrobial resistance in *Aspergillus fumigatus*

Anna E. Lehmann[1], Enrique Aguilar Ramírez[2], Nancy P. Keller[2], and Joseph Heitman[1*]

[1]Department of Molecular Genetics and Microbiology, Duke University School of Medicine, Durham, NC, USA

[2]Department of Medical Microbiology and Immunology, University of Wisconsin – Madison, Madison, WI, USA

*Corresponding author: Joseph Heitman

Email: heitm001@duke.edu

**Highlights**

- *A. fumigatus* rapidly gains and loses chromosomes in response to antimicrobial stress.
- Aneuploidy leads to large-scale transcriptional and metabolic changes.
- Overexpression of *nscR* is sufficient to confer FK506 tolerance in the euploid.
- Aneuploidy reduces susceptibility to both FK506 and azole antifungals.

**Summary**

Aneuploidy causes genome plasticity and enables adaptive responses that confer drug resistance in eukaryotes ranging from fungal pathogens to human cancer cells. *Aspergillus fumigatus* is a soil-resident fungus and the most common cause of invasive fungal infections globally. Aspergillosis has an alarmingly high mortality rate due in part to treatment failure resulting from widespread antimicrobial resistance and an ability of the fungus to dynamically adapt to changing environmental and host conditions. Our understanding of these treatment failures is hindered by gaps in knowledge about how this organism adapts to resist antimicrobial stress. We find that exposure to FK506, an antifungal and immunosuppressive compound produced by *Streptomyces*, selects for whole-chromosome aneuploidy in this fungus. Growth without FK506 results in rapid aneuploid chromosome loss and reversion to the euploid, drug-susceptible state. These chromosome duplications also reduce susceptibility to clinically-used azole antifungals, underscoring the utility of aneuploidy as a dynamic stress adaptation strategy. Transcriptomic analysis revealed that Chr7 disomy leads to induction of the normally-silent neosartoricin biosynthetic gene cluster in response to FK506 exposure, and we demonstrate that constitutive genetic induction of this cluster recapitulates in the euploid background the response to FK506 in the aneuploid state. We further show that this response is independent from the production of neosartoricin, suggesting a role for cross-pathway metabolic changes resulting from activation of this gene cluster or from the aneuploid state. This study represents a major advance in understanding how aneuploidy leads to transient adaptation and antimicrobial drug resistance in a global human fungal pathogen.

**Keywords:** *Aspergillus fumigatus*, antimicrobial resistance, aneuploidy, secondary metabolism

## Introduction

Aneuploidy, an abnormal complement of whole chromosomes or chromosome segments, is a conserved adaptive strategy across eukaryotes. Whole-chromosome and segmental aneuploidies are ubiquitous in human cancers and are hypothesized to enhance tumor survival and proliferation in a dynamic and context-specific manner by altering gene dosage and activating generalized stress responses (reviewed in[1–3]). Aneuploidy is also an important persistence strategy in single-celled eukaryotes. In yeast, unstable aneuploidy can serve as a rapidly-acquired, temporary solution to diverse stressors that potentially provides an avenue to less deleterious, stable genetic change[4–8]. Aneuploidy is also known to underlie unstable stress adaptation in multiple human and plant fungal pathogens[9]. Significantly, aneuploidy can serve as a major cause of reduced susceptibility to triazoles, the primary antifungal class administered clinically. In *Candida albicans*, azole resistance results from isochromosome formation of the left arm of Chr5, which harbors the genes that encode

the azole target enzyme Erg11 and the drug efflux pump-activating transcription factor Tac1[10–12]. Whole-chromosome aneuploidy has also been reported as an antifungal resistance strategy in the pathogenic yeast *Cryptococcus neoformans*[13,14] and the plant pathogen *Aspergillus flavus*[15]. Additionally, a recent report identified segmental duplications of regions encoding the azole target genes *cyp51A* and *cyp51B* in azole-resistant *Aspergillus fumigatus* clinical isolates, suggesting a correlation between copy number variation and clinically-relevant antifungal resistance in this ubiquitous global pathogen[16]. These observations support a broadly conserved role for aneuploidy in stress adaptation in pathogenic fungi. Despite the apparent conservation of this phenomenon, however, genomic plasticity as a means of antifungal resistance remains unexplored in many prominent human and plant pathogens.

*A. fumigatus* is a globally-distributed, soil-resident fungus and the leading cause of invasive fungal infections worldwide[17]. This organism has evolved a range of strategies that allow it to persist in its harsh and highly variable ecological niche, and this same suite of adaptive traits contribute to its pathogenicity. One such adaptation is the inducible production of secondary metabolites, two of the most well-studied being 1) DHN melanin, which protects conidia from UV radiation and reactive oxygen species and inhibits host cell apoptosis[18–20] and 2) gliotoxin, which is toxic to mammalian host cells[21–24]. Various other secondary metabolites exhibit both antimicrobial activity against soil microbes and cytotoxic activity against host immune cells, suggesting context-dependent and evolutionarily-relevant reasons for their maintenance in the genome and selective induction (reviewed in[25,26]). The genes involved in secondary metabolite biosynthesis are encoded in self-contained and spatially discrete biosynthetic gene clusters (BGCs), which are often transcriptionally inactive under standard culture conditions[27]. Difficulties in activating silent BGCs have hindered efforts to elucidate the functions of these enzymes and products in fungal physiology and adaptation. Induction of BGCs is further complicated by the often observed endogenous cross-talk of metabolites within a species. Several instances have been observed in *A. fumigatus* ranging from loss of one metabolite (e.g. fumigaclavine C or hexadehydroastechrome) resulting in an increase in production of another metabolite (fumitremorgins)[28,29], evidence of an enzyme from one BGC active in synthetic potential in another BGC[30], and changes in BGC gene expression upon deletion of genes in a different BGC[31].

Recent efforts undertaken to activate normally-silent BGCs have employed co-culture with soil microbes including *Streptomyces* and other Aspergilli that co-occupy a saprophytic environmental niche[32–34]. Several such studies have resulted in the identification of new natural products, suggesting a role for these compounds in cross-talk and interaction with other, potentially competing microbes[32,33,35–38]. The specific induction of BGCs in response to microbes that co-occupy an environmental niche supports their role in defense against competitors and illustrates the diverse

and complex strategies utilized by this organism to adapt to external stress and the important role that context-dependent gene activation and silencing can have.

Despite the apparent ubiquity of aneuploidy as a rapidly-acquired, flexible persistence strategy in eukaryotes, the potential roles of aneuploidy in *A. fumigatus* adaptation to environmental and infection-relevant stresses remains a significant gap in knowledge. Here, we identify whole-chromosome aneuploidy formation in *A. fumigatus* in response to the bacterial natural product and immunosuppressant FK506. We demonstrate that Chr7 duplication induces transcription of the neosartoricin (*nsc*) BGC, which is silent under normal culture conditions. Induction of this cluster in a euploid background is sufficient to alter the response to FK506 in a manner consistent with that observed in Chr7 aneuploids, but independent of neosartoricin production, suggesting a broader role for this gene cluster in globally altering secondary metabolite biosynthetic processes. Additionally, the aneuploid chromosome duplications reduce susceptibility to azole antifungals and result in subpopulations of cells able to survive at supra-MIC drug concentrations. These results extend our knowledge of aneuploidy as a conserved adaptive strategy in eukaryotes to the important fungal pathogen *A. fumigatus*, revealing novel strategies utilized by this organism to persist in the face of antimicrobial stress.

## Results

### *Unstable aneuploidy alters FK506 hyphal growth inhibition in the* A. fumigatus *reference strain A1163*

Our previous work has utilized FK506, an antimicrobial and immunosuppressive compound produced by *Streptomyces*, to uncover stable and unstable genetic adaptive strategies in fungal pathogens including *Mucor*[39,40] and *Cryptococcus*[41–43] spp. FK506 binds to the endogenously-expressed protein FKBP12 and forms a complex that inhibits the protein phosphatase calcineurin, a mechanism that is broadly conserved across eukaryotes[44–46]. In many fungi, FK506 is an ideal model compound with which to study genetic and epigenetic mechanisms of acquired antimicrobial resistance because overcoming calcineurin inhibition results in a clear and binary phenotypic switch, from no growth to growth in *Cryptococcus*[41–43] and a dimorphic switch between yeast and hyphal growth in *Mucor*[40,47]. In *A. fumigatus*, calcineurin inhibition by pharmacologic or genetic means impacts a host of processes including development and morphology of conidia (asexual reproductive particles), hyphal extension, branching, septation and polarized growth, and cell wall composition[48–52]. The result of these severe growth and morphological defects is an abolition of virulence in pathogenesis models, underscoring the essentiality of calcineurin-mediated processes to the pathogenic capabilities of this organism[49]. Complete reversal of these FK506-dependent phenotypes has only been observed by genetic mutation of the drug target-encoding gene *fkbp12-1*[53]. It is likely that other single-gene mutations are insufficient to completely bypass calcineurin activity because

calcineurin controls multiple discrete cellular processes via independent pathways (reviewed in[54,55]). Therefore, we elect to assess FK506 tolerance as an improvement of growth in one or more, rather than necessarily all, phenotypes resulting from calcineurin inhibition.

To understand how *A. fumigatus* adapts to resist calcineurin inhibition by FK506, we employed a screen similar in design to those with which we previously identified both RNAi-dependent epimutations silencing the FKBP12 mRNA transcript and stable mutations in *fkbA* in *Mucor*[40] and stable mutations in calcineurin bypass genes in *Cryptococcus*[42]. We hypothesized that we could identify stable or unstable mutations in *fkbp12-1*, which would lead to a phenotype indistinguishable from that of wild-type grown without FK506, and/or in calcineurin pathway genes. Conidia were plated on medium containing FK506 at a concentration of 1 µg/mL, which severely impairs radial growth of the wild-type (Fig. 1*A*). Colonies that exhibited increased radial mycelial growth were isolated and single-spored. A total of 52 FK506-resistant isolates were obtained, none of which had completely restored growth similar to that which would be expected as a result of *fkbp12-1* mutation. Whole-genome sequencing of these isolates revealed that they were predominantly whole-chromosome aneuploids (34/52), with an additional 14 isolates having identifiable stable mutations in potential calcineurin bypass genes (Fig 1*B*; Table S1). We did not identify any isolates with mutations in *fkbp12-1* or the calcineurin catalytic or regulatory subunits *cnaA* or *cnaB*. Forthcoming studies will further explore the *crzA*-dependent and -independent roles of these genes in the calcineurin pathway. We elected to focus the bulk of our subsequent study on Chr7 aneuploids for several reasons. First, Chr7 aneuploids undergo clear and specific phenotypic changes in FK506 susceptibility compared to wild-type, which are amenable to identifying correlative genetic changes directly related to the aneuploid response to FK506. Second, Chr7 is the smallest chromosome, meaning that transcriptional alterations due to copy number increases but unrelated to resistance are likely to be minimized relative to isolates with a full duplication of Chr4 or Chr6. Third, Chr7 disomy was the second-most frequently observed aneuploid karyotype in our screen, indicating its potential to be well-tolerated and important to the drug response.

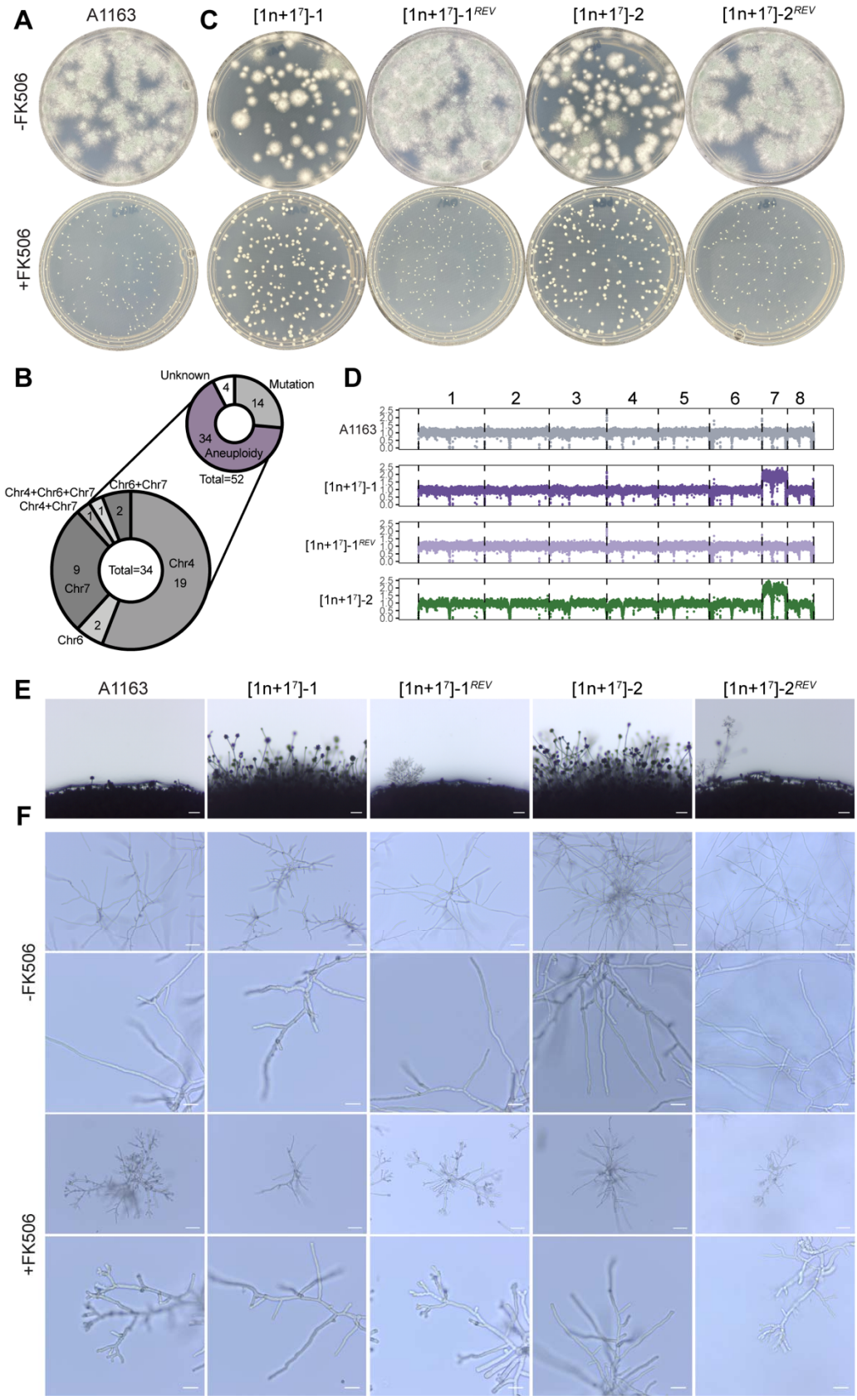
A
A1163
C
[1n+1^7]-1
[1n+1^7]-1^REV
[1n+1^7]-2
[1n+1^7]-2^REV
-FK506
+FK506
B
Unknown
4
Mutation
14
34
Aneuploidy
Total=52
Chr4+Chr6+Chr7
Chr4+Chr7
Chr6+Chr7
1
1
2
9
Chr7
Total=34
Chr4
19
2
Chr6
D
1
2
3
4
5
6
7
8
A1163
[1n+1^7]-1
[1n+1^7]-1^REV
[1n+1^7]-2
E
A1163
[1n+1^7]-1
[1n+1^7]-1^REV
[1n+1^7]-2
[1n+1^7]-2^REV
F
-FK506
+FK506

157

**Figure 1. Aneuploidy confers FK506 resistance.** (*A*) A1163 WT growth on AMM – (top) or + (bottom) 1 µg/mL FK506 for 3 days at 37°C. (*B*) Distribution of aneuploidies, high- or medium-impact mutations, and unknown mode of resistance determined from analysis of WGS data from FK506-resistant isolates. Zoomed out pie chart shows frequency of chromosome duplications in the set of 34 unstable aneuploids. (*C*) 2 representative Chr7 aneuploids grown on AMM + 1 µg/mL FK506 for 3 days before (top) and after (bottom) passage on drug-free AMM. Representative images from ≥ 3 biologically independent replicates. (*D*) Normalized read depth averaged over 500 bp intervals plotted across the genome for A1163 euploid and the aneuploids in (*C*). (*E*) $10^5$ conidia were spotted on AMM + 1 µg/mL FK506 and grown at 37°C for 2 days. Microscopy images of hyphal growth at the colony edge are representative of 3 biologically independent replicates. Scale bar indicates 100 µm. (*F*) Conidia were inoculated in AMM +/- 1 µg/mL FK506 in a microscopy growth chamber and grown at 37°C for 24 hours. Scale bars indicates 50 µm (top) and 20 µm (bottom). Representative images from ≥ 3 biological replicates.

We next assessed the stability of the aneuploid chromosome duplications in the absence of FK506 selection. Aneuploids were cultured on drug-free medium for 9 days, during which conidia from the perimeter of the colony were patched to a new drug-free plate every 3 days. After drug-free passage, conidia were re-plated on FK506 medium and assessed for loss or retention of the original hyphal growth phenotype. Passage on drug-free medium led to rapid loss of the FK506 resistance phenotype, indicating that aneuploids are highly unstable in the absence of selective pressure (Fig. 1*C*). Sequencing of the reverted (*REV*) isolate showed a corresponding loss of the aneuploid chromosome, directly linking FK506 tolerance to aneuploidy (Fig 1*D*; Table S1). At the beginning of this study, we identified 6 isolates that originated from a single initial pool of conidia but formed separate resistant colonies on individual FK506 selection plates. Whole-genome sequencing of these isolates revealed that all 6 carried an extra copy of Chr7 and differed from the progenitor strain by several identical SNPs in coding regions of the genome (Table S1). Based on the genetic and ploidy similarities, we hypothesize that these isolates originated from a clonal population of Chr7 aneuploids in the initial pool of conidia. This result suggests that aneuploidy exists at a low baseline frequency in conidial populations, and that chromosome duplications can be maintained in the presence of a stress such as FK506 if they provide a fitness benefit. Due to their apparent clonality, these 6 Chr7 aneuploid isolates are treated as a single independent event ($[1n+1^7]$-1) in all results presented here. To avoid identifying additional clonal isolates, and to confirm that the additional SNPs present in the aneuploids are not responsible for the aneuploid karyotype, all other isolates described in this study were isolated from 20 different single-spore derived populations of conidia from the original A1163 stock, and one resistant colony was isolated per replicate.

On solid medium with FK506, the euploid lacks radial growth of conidiophores or hyphae (Fig. 1*E*). In contrast, Chr7 aneuploids exhibit restored conidiophore growth compared to euploid, and this phenotypic change is lost following passage on drug-free medium (Fig. 1*E*). Consistent with previously-described effects of calcineurin inhibition, we observed inhibition of normal hyphal extension and polarity, indicated by increased density of hyphae, stunted extension, and aberrant branching at the apical tips, in the euploid +FK506 (Fig. 1*F*, leftmost panel). In contrast, Chr7 aneuploids lack the hyper-branched tips observed in the euploid, and these phenotypes are reversed to a state that is indistinguishable from wild-type in the reverted strains (Fig. 1*F*). These results directly implicate Chr7 aneuploidy in the reversal of these calcineurin-dependent growth and morphological phenotypes.

*Chr7 aneuploidy leads to increased expression of secondary metabolite biosynthetic genes*

We next sought to determine if specific transcriptional changes confer FK506 resistance in Chr7 aneuploids. To probe a potential transcriptional basis for the observed phenotypic changes, we conducted 2 independent RNA sequencing experiments with the euploid and independent Chr7

aneuploids, [1n+1$^{7}$]-1 and [1n+1$^{7}$]-2, with and without FK506. Total RNA was extracted from triplicate cultures and analyzed by paired-end bulk mRNA sequencing (Materials and Methods). Parallel DNA sequencing from [1n+1$^{7}$]-1 cultured under the drug-free RNA extraction condition confirmed that the chromosome duplication was maintained in the drug-free condition (Fig. S1*A*). RNA-seq reads were mapped to the A1163 reference genome[56]. PCA was performed analyzing the top 1000 variable transcripts in each experiment, which capture the majority of variance in the data (Fig. S1*B, C*). In both cases, most of the variance was explained in principal components 1 and 2 (Fig. S1*D, E*). PCA indicates that for [1n+1$^{7}$]-1, drug condition is the primary factor explaining gene expression differences (PC1; 52% of variance), followed by ploidy (PC2; 22% of variance) (Fig. 2*A*; Fig. S1*D*). In contrast, in [1n+1$^{7}$]-2, variance is primarily driven by ploidy (PC1; 61%), with drug condition explaining 19% of the observed variance (Fig. 2*B*; Fig. S1*E*). Analysis of differentially expressed genes between aneuploids and euploid +FK506 revealed large-scale changes in gene expression, with 291 upregulated and 716 downregulated genes in experiment 1 and 1537 upregulated and 2093 downregulated genes in experiment 2 (Fig. 2*C, D*; Table S2). These differences in are consistent with the PCA results, illustrating a much larger effect of aneuploidy on the global transcriptome in [1n+1$^{7}$]-2 than in [1n+1$^{7}$]-1.

We observed that the transcription factor *nscR* is significantly differentially expressed between 9- (experiment 1) and 11.5- fold (experiment 2) in Chr7 aneuploids +FK506 relative to euploid (Fig. 2*C, D*; Table S2). This transcription factor controls expression of the genes in the neosartoricin (*nsc*) BGC (also called the fumicycline BGC[33]). The *nsc* BGC, located near the left telomere of Chr7, is responsible for the production of the secondary metabolite neosartoricin[57]. This gene cluster, with the exception of the FAD-dependent monooxygenase *nscC*, is silent or lowly expressed in the euploid and Chr7 aneuploids -FK506, and minimally induced in the euploid +FK506 (Fig. *2E, F*). FK506 exposure induces *nsc* gene expression specifically in the aneuploids, with *nscR* having the highest expression (Fig. 2*F*).

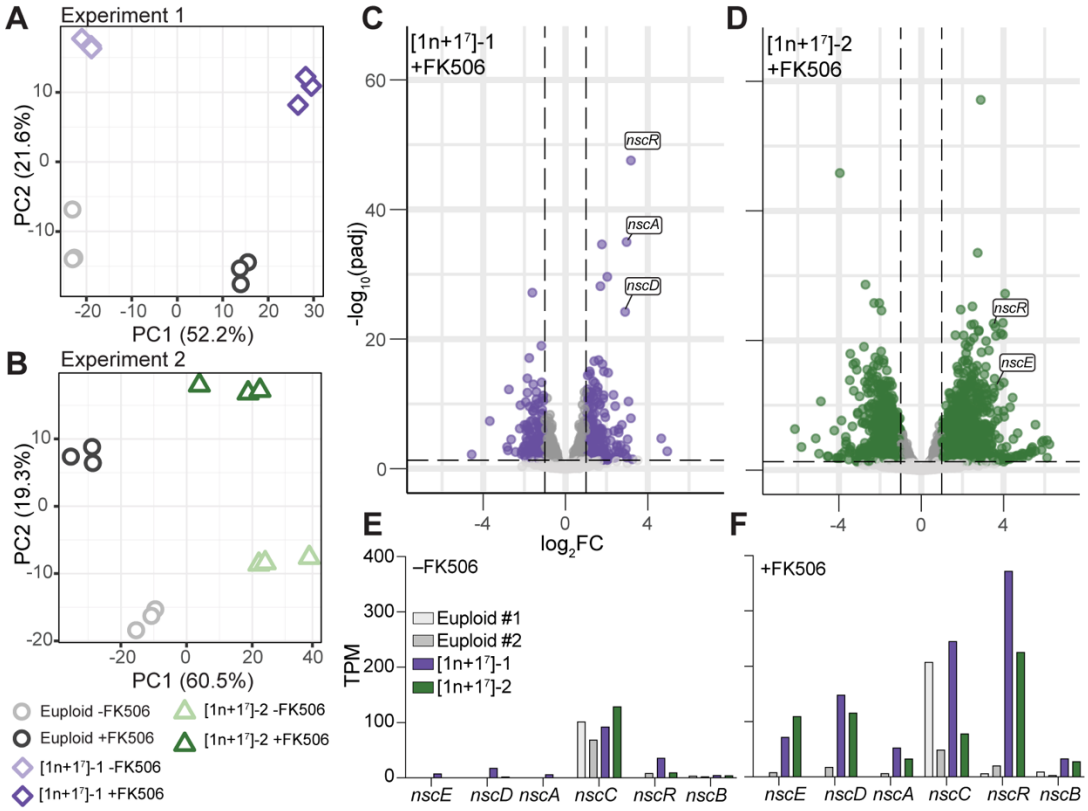


**Figure 2. Neosartoricin biosynthetic genes are induced in Chr7 aneuploids +FK506.** (*A* and *B*) PCA of the top 1000 most variable genes from 2 independent RNA-seq experiments with aneuploids [1n+1$^7$]-1 (Experiment 1) (*A*) and [1n+1$^7$]-2 (Experiment 2) (*B*). (*C* and *D*) Differentially expressed genes in comparison between Chr7 aneuploid +FK506 and WT +FK506 in experiment 1 (*C*) and 2 (*D*). Dashed lines indicate $\log_2$FC = ±1 and $p_{adj}$ = 0.05. (*E* and *F*) Average TPM in euploid and Chr7 aneuploids -FK506 (*E*) and +FK506 (*F*). Bar graphs indicate average (mean) TPM from 3 technical replicates.

Secondary metabolite BGCs can be transcriptionally activated by both pathway specific transcription factors and global regulators or epigenetic modifications that themselves are induced by various environmental stimuli[58–60]. Given the magnitude of transcriptional changes observed in the aneuploids, we sought to determine whether aneuploidy globally alters secondary metabolite BGC transcription or whether the effect is specific to the *nsc* BGC. To address this question, we quantified TPMs for the 18 additional known A1163 secondary metabolite BGCs[61] and observed that these clusters were either silent in all conditions or did not undergo the same differential change as neosartoricin in response to aneuploidy and FK506 (Fig. S2). Notably, the fumagillin BGC monooxygenase *fmaE* (AFUB_086100) was constitutively highly expressed, and several genes in the hexadehydroastechrome and trypacidin BGCs undergo increased induction in response to FK506. Unlike the *nsc* BGC, however, most genes in these clusters remained silent. Taken together, these results indicate that aneuploidy of Chr7 leads to induction of *nsc* BGC expression specifically in response to FK506 exposure, and that this induction occurs at a higher level than would be expected solely based on copy number changes. We discuss the implications of this in the context of bistable switch models in the discussion below.

nscR *overexpression confers FK506 resistance*

To directly explore a potential role for the *nsc* BGC in the aneuploid phenotypes observed in response to FK506, we generated a strain expressing *nscR* (AFUB_086680) under control of the *A. fumigatus* Af293 *gpdA* promoter in the A1163 euploid background (*nscR*$^{OE}$). The *nscR* transcript is constitutively overexpressed approximately 75 to 100 fold in this strain (Fig. 3*A*). Microscopic observation of growth at the colony edge on solid medium +FK506 shows increased conidiophore growth in *nscR*$^{OE}$ (Fig. 3*B*). Rather than forming long and sparse filaments like those observed in the aneuploid, however, *nscR*$^{OE}$ forms a dense mat of conidiophores concentrated closer to the colony edge. In liquid culture, *nscR*$^{OE}$ exhibits decreased hyperbranching similar to Chr7 aneuploids (Fig. 3*C*). These observations indicate that *nscR* overexpression alleviates FK506-dependent hyphal growth and conidiation defects in a manner similar to Chr7 aneuploidy. We hypothesize that the phenotypic differences between Chr7 aneuploids and *nscR*$^{OE}$ in response to FK506 could result from additional, aneuploidy-dependent transcriptional changes as well as the differences in *nscR* expression between aneuploids and *nscR*$^{OE}$. Nevertheless, our findings indicate that overexpression of a single gene largely recapitulates the aneuploid response to this specific stressor in a euploid background.

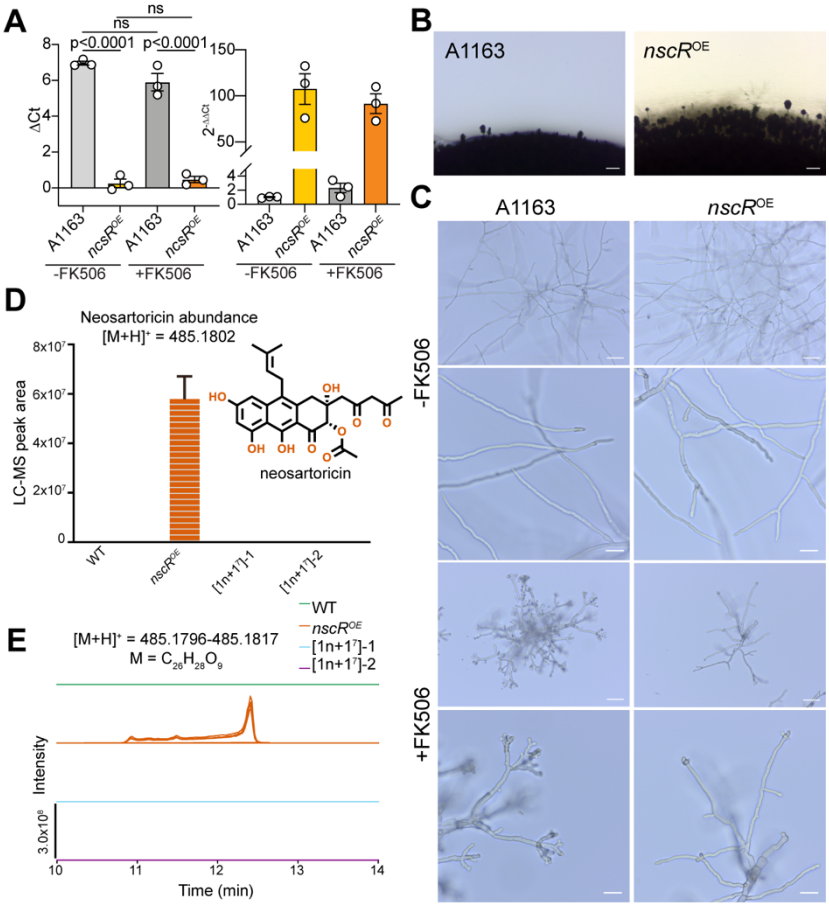


**Figure 3. *nscR* overexpression confers FK506 resistance.** (*A*) Fold change values of *nscR* transcript in WT and *nscR*$^{OE}$ strains +/-FK506 relative to WT untreated. RNA was extracted from 16-hour cultures seeded at $10^6$ spores/mL in liquid AMM +/- 1 µg/mL FK506 and grown at 37°C with shaking at 200 rpm. ΔCt values were calculated by normalizing to *act1* and ΔΔCt values relative to WT untreated. Points indicate biological replicates and are represented as averages of 3 technical replicates; error bars indicate SEM. Statistical test: one-way ANOVA with Tukey's multiple comparison test. (*B*) $10^5$ conidia were spotted on AMM + 1 µg/mL FK506 and grown at 37°C for 2 days. Microscopy images of hyphal growth at the colony periphery are representative of 3 biologically independent replicates. Scale bar indicates 100 µm. (*C*) Conidia were inoculated in AMM +/- 1 µg/mL FK506 in and grown at 37°C for 24 hours. Scale bar indicates 50 µm (top) and 20 µm (bottom). Representative images from 3 biologically independent replicates. (*D*) Abundance of neosartoricin in the different strains, determined based on the average area under the curve of the detected peak for the molecular ion [M+H]+ = 485.1802 across the four replicates analyzed, and (*E*) its associated chromatogram.

*Aneuploid secondary metabolite profiles distinguish them from wild type and* nscR$^{OE}$

To directly investigate a correlation between *nscR* expression and neosartoricin production in Chr7 aneuploids and *nscR*$^{OE}$, we profiled the metabolites produced in these strains by LC-MS. Surprisingly, we found that only *nscR*$^{OE}$ produces neosartoricin, while this compound is absent or at such levels to be undetectable in Chr7 aneuploids (Fig. 3*D, E*). Considering the many instances of metabolite cross-talk in *A. fumigatus*, we performed a targeted metabolomics analysis to assess the abundance of well-characterized secondary metabolites of *A. fumigatus* across the WT, *nscR*$^{OE}$, and Chr7 aneuploid strains. This analysis revealed a pronounced increase in pyripyropene A biosynthesis (Fig. 4*A*) in the aneuploid strains, along with clear increases in fumitremorgin C, pseurotin A, and fumagillin (Fig. S3).

When all LC-MS features associated with *A. fumigatus* metabolites were considered, their relative abundance across strains was compared by principal component analysis (PCA). The resulting chemical profiles segregated into three distinct groups (Fig 4*B*): WT, *nscR*$^{OE}$, and the Chr7 aneuploids, indicating that, at a global level, the aneuploids display a chemical profile clearly distinct from both *nscR*$^{OE}$ and the WT strain. To further elucidate how the aneuploids differ from WT, we conducted a volcano plot analysis using the LC-MS features (Fig 4*C*). This revealed that a large number of metabolites were overproduced in the aneuploids relative to WT. Interestingly, many of these metabolites were consistent with ergosterol-type triterpenes, based on their fragmentation patterns and predicted formulas (Fig. S4). Notably, fumitremorgin C was overproduced in both aneuploids as well as in the *nscR*$^{OE}$ strain (Fig 4*D*).

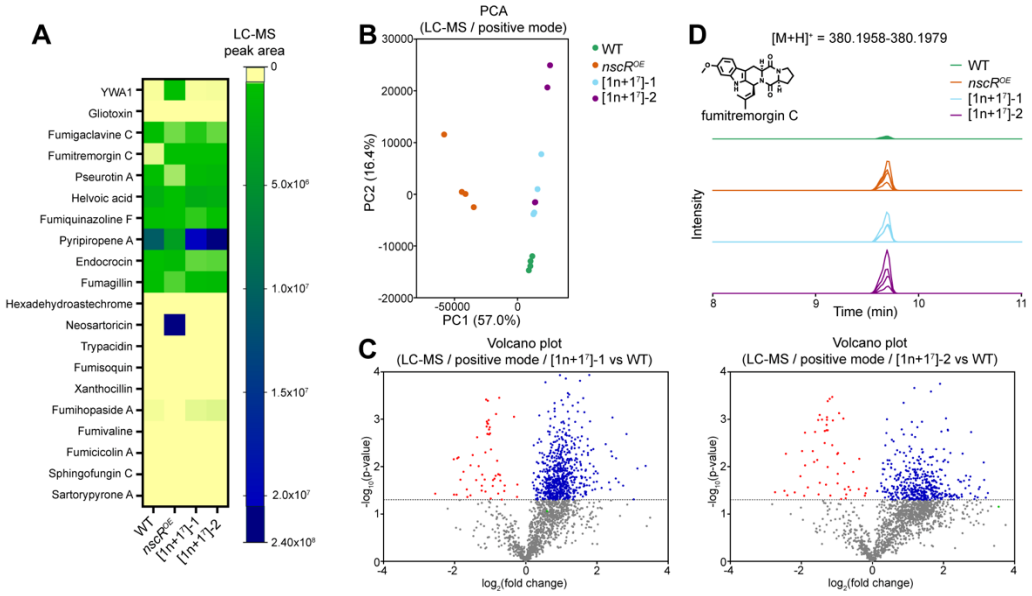


**Figure 4. Secondary metabolite profiles of aneuploids.** (*A*) Heatmap representing the abundance of well-characterized secondary metabolites of *A. fumigatus*, based on the average area under the curve associated with their LC-MS features. (*B*) Principal component analysis (PCA) showing the variance among the different strains according to the abundance of all LC-MS–detected features in positive mode. (*C*) Volcano plots comparing the abundance of detected features (in positive mode) between the aneuploid [1n+1$^7$]-1 and the WT strain, as well as between the aneuploid [1n+1$^7$]-2 and the WT strain (the feature corresponding to fumitremorgin C is highlighted in green). (*D*) Stacked chromatograms of fumitremorgin C displaying its abundance across the WT, *nscR*$^{OE}$, [1n+1$^7$]-1 and [1n+1$^7$]-2 strains. Four replicates were included in all the representations.

*Aneuploidy alters azole susceptibility*

Segmental duplications of genomic regions encoding *cyp51A* (Chr4), *cyp51B* (Chr7), and the *cyp51* electron carrier protein *cyp51ec* (Chr5) have been correlated with elevated azole resistance in *A. fumigatus* clinical isolates[16]. Increased expression of *cyp51A* via promoter mutations is also an established azole resistance mechanism in *A. fumigatus*[62–68]. Azole antifungals are direct inhibitors of the ergosterol biosynthetic enzyme Cyp51A, and Cyp51B is a parallel biosynthetic enzyme that is not a direct target of the drug but has been suggested to have a role in compensating for loss of Cyp51A activity in azole-resistant isolates[69]. Given the predominance of Chr4 and Chr7 disomies in our dataset, we next investigated whether these chromosome duplications could affect azole susceptibility. We employed E-tests to measure the voriconazole MICs of aneuploids and reverted isolates and observed that aneuploids with Chr7 duplications have decreased voriconazole susceptibility (Fig. 5*A, B*). Interestingly, duplication of Chr4 has no effect on E-test MIC, but duplication of Chr4 and Chr7 together increased the MIC almost twofold compared to duplication of Chr7 alone. We also measured MICs for 2 other azoles, isavuconazole and posaconazole, for Chr7 aneuploids and observed a subtle decrease in susceptibility to these compounds consistent with the trends observed with voriconazole (Fig. S5). Several aneuploids also gave rise to subpopulations of cells able to grow at supra-MIC drug concentrations inside the zone of inhibition. This result suggests that aneuploidy could promote elevated rates of acquired azole resistance, either stable or unstable. With the exception of [1n+3[4,6,7]], for which the MIC did not change, passaged, FK506-susceptible isolates had MICs comparable to that of the euploid. We hypothesize that the elevation in MIC observed in some of the passaged isolates could be due to residual aneuploid populations that could be selected for under azole stress. We also measured MICs by CLSI broth dilution method with RPMI medium and observed a somewhat different pattern than the E-test results, with [1n+1[4]] and [1n+2[6,7]] having the highest MICs (Fig. 5*C*). These results underscore the important physiological differences that may occur under different growth conditions (nutrient content of the medium and culture on solid medium vs. submerged culture) and highlight the differing roles aneuploidy can have in antifungal responses under these distinct conditions.

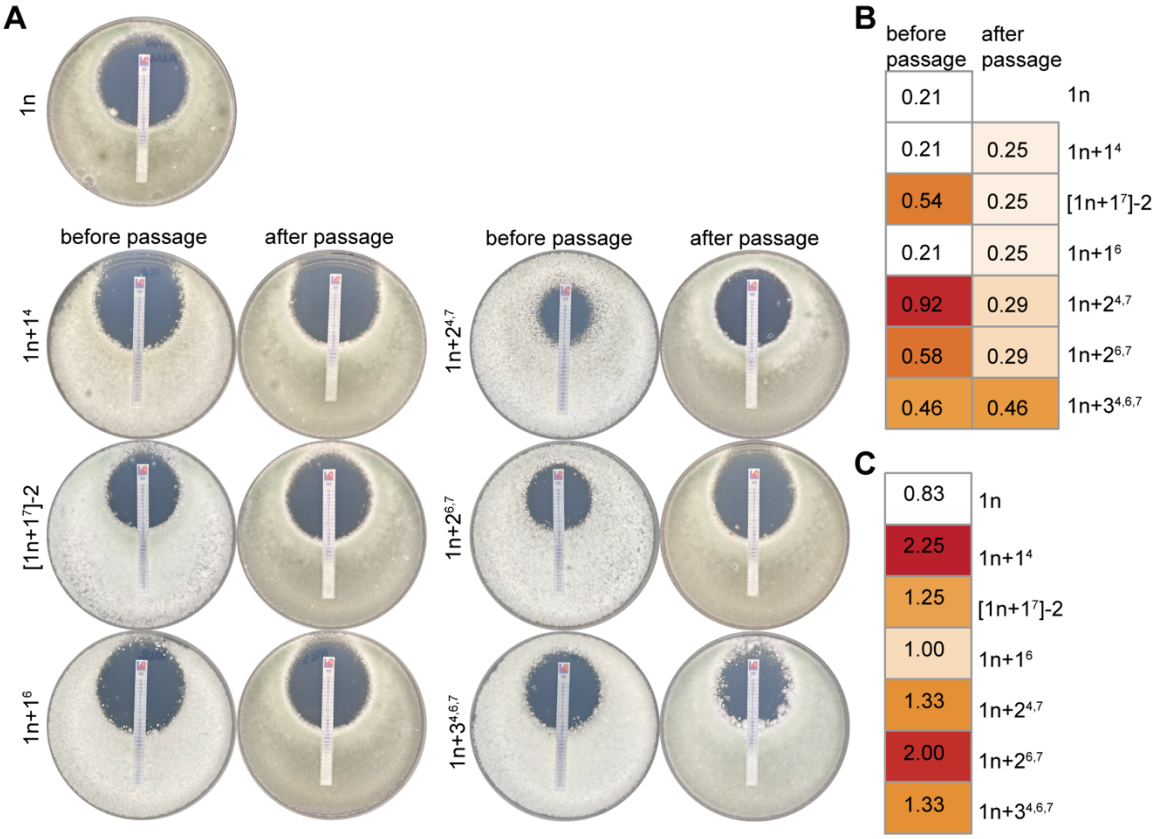


**Figure 5. Aneuploidy reduces voriconazole susceptibility.** (*A*) Representative images of voriconazole E-test MICs of aneuploids before and after passage on drug-free medium. (*B*) Average MICs (µg/mL voriconazole) from 3 biological replicates for strains in (*A*). (*C*) MICs (µg/mL voriconazole) measured by CLSI broth dilution; averages of 3 to 4 biological replicates.

## Discussion

Aneuploidy functions as a transient adaptive strategy in eukaryotes from fungi to humans, allowing for rapid adaptation to a range of stresses in a genetically impermanent and readily-reversible manner. Here, we illustrate the versatility of unstable aneuploidy in *Aspergillus fumigatus* in adapting to FK506, a calcineurin-inhibiting natural product produced by *Streptomyces*, and azole antifungals, synthetic compounds that inhibit the critical ergosterol biosynthetic enzyme Cyp51A. Our identification of 6 clonal Chr7 aneuploids promoting increased hyphal growth on FK506 medium indicates that aneuploidy was likely present in the starting population of conidia, which were harvested from drug-free medium, and did not occur in response to FK506. The fact that aneuploidy likely arose under non-stressful conditions suggests that genomic instability can function to increase diversity within a population and increase the odds of beneficial adaptation under stress.

We observed that aneuploidy is a major form of adaptation reducing the conidiophore growth inhibition and hyphal polarity defects caused by FK506. The specific morphological traits affected vary between aneuploids, with some primarily increasing conidiophore formation and others reducing hyperbranching and polarity defects at the hyphal tips. Calcineurin is known to mediate a host of cellular functions in *Aspergillus* including conidiation, hyphal growth, and cell wall structure[48–52].The phenotypic differences between aneuploids in response to calcineurin inhibition may point to specific calcineurin-dependent processes and indicate that different aneuploidies may modify distinct processes in response to the same inhibitor. The diverse processes in *A. fumigatus* influenced by calcineurin remain incompletely characterized, and studying the changes in the FK506 response in aneuploids can provide insight into different ways in which calcineurin controls cellular physiology. As calcineurin is critical to the ability of this fungus to cause disease[49,50], understanding calcineurin function is important for understanding the success of *A. fumigatus* as a human pathogen.

In this study, we investigated transcriptional changes in Chr7 aneuploids, which exhibit increased conidiophore formation, decreased hyperbranching, and normal polarity at the apical hyphal tips. We found that the normally-silent *nsc* BGC is specifically activated in aneuploids exposed to FK506, and induction of this cluster results in increased conidiophore formation and reversal of the hyperbranching phenotype caused by FK506. These effects are independent of neosartoricin production. Interestingly, deletion of the calcineurin-activated transcription factor *crzA* is also reported to increase *nsc* gene expression but not neosartoricin production[71]. In fact, several studies have shown that BGC transcript abundance does not always translate to concomitant metabolite production[72,73]. The mechanisms underlying non-concordance between transcript and metabolite production is understudied but could involve post-transcriptional and/or post-translational modifications such as phosphorylation regulation of AflR, the pathway specific transcription factor required for sterigmatocystin and aflatoxin production[74].

Our observations of a neosartoricin-independent function for *nscR* in the response to FK506 point to potential additional cellular functions of this transcriptional regulator, whose only previously-known function is neosartoricin biosynthesis. Several studies have demonstrated that transcription factors encoded within one BGC can regulate the expression of secondary metabolite genes in other BGCs, often those located on other chromosomes. For example, in *A. fumigatus*, HasA both positively and negatively regulates multiple BGCs[75], in *Penicillium expansum*, XanC specifically activates the citrinin BGC[76], and in *Aspergillus nidulans*, ScpR drives expression of both the *inp* BGC and the asperfuranone BGC[72]. Similarly, in *Fusarium graminearum*, TRI6 not only activates the trichothecene BGC but also influences genes involved in the isoprenoid/mevalonate pathway[77]. Additionally, the broad changes in metabolite production in aneuploids indicate that ploidy changes have global effects on metabolism, and it is therefore conceivable that *nsc* pathway-independent effects could influence adaptation in other contexts. These observations bolster the assertion that aneuploidy is a versatile adaptive mechanism with beneficial selective potential in diverse environments. Because *A. fumigatus* has a broad global distribution and is able to survive in varied and often harsh environments, this hypothesis is in line with this pathogen's evolutionary necessity to persist under a dynamic range of adverse conditions.

Our studies revealed that aneuploidy-driven activation of the otherwise silent *nsc* BGC involved dramatic activation of *nscR*, which encodes the transcription factor that activates expression of this gene cluster. That the extent of *nscR* activation (9 to 11.5-fold) is well beyond the 2-fold induction one might expect in an aneuploid with one additional chromosome (1n+1) suggests that NscR action on its own promoter may underlie this markedly increased gene activation. Transcription factors that activate their own gene expression are often critical components of so-called bistable switches, in which the level of gene and its targets is low in one stable state, and dramatically elevated in the other stable state. For instance, several studies demonstrate that the aflatoxin transcription factor AflR binds to its own promoter, possibly to balance in its broader regulatory functions in development and overall cellular metabolism[78–80]. Another prime example is the white to opaque switch, which occurs in *C. albicans* and serves to activate mating fertility in the opaque state[81–84]. The white to opaque transition is driven by the transcription factor Wor1, which acts on the promoters of downstream effectors governing the morphotype transition as well as on its own promoter in a positive feedback loop[84,85]. This all-or-nothing transcriptional activation means that expression of Wor1 is very low in white cells, and very high in opaque cells[86,87]. Our findings suggest that aneuploidy could be one mechanism by which biosynthetic gene clusters that can operate as bistable switches might be activated and selected for during environmental stress. On a more general level, this finding suggests that we might be able to systematically activate biosynthetic gene clusters by isolating or constructing aneuploid strains to similarly activate encoded bistable switches.

In the context of intra-population genetic diversity, increased copy number of full chromosomes may increase the odds of positive selection compared to stable genetic mutations by flexibly altering large set of genes rather than a single gene. The advantages of this flexibility are demonstrated by our results that the same aneuploid strains have adaptive advantages in the context of both FK506 and azole antifungals. Given the variability in stress conditions encountered by *A. fumigatus* both in its environment and during host interactions, it is conceivable that aneuploidy could facilitate rapid adaptation and persistence in both ecological and disease contexts through transcriptional changes that can be turned on and off without the need for permanent genetic change. In human cancers, aneuploidy can serve as both a temporary drug resistance strategy by altering gene dosage and as a driver of permanent genetic change by promoting chromosomal rearrangements. We observed that aneuploids give rise to subpopulations that are resistant to high azole concentrations in a manner not observed in the euploid. Because it is known that increased expression of *cyp51A* can cause azole resistance[68,88], one hypothesis to explain these observations is that a doubling in *cyp51A* copy number in Chr4 aneuploids could increase expression of this gene, through increased copy number and perhaps an increased mutation rate at this locus, leading to an increased rate of acquired voriconazole resistance. This is analogous to the known role of changes in *ERG11* gene copy number in conferring azole resistance as a result of aneuploidy in *C. albicans*[10,89] and *C. neoformans*[13,14]. Future work will involve characterizing the ploidy and genetic differences between these resistant subpopulations and their aneuploid parents.

One limitation of our study is that it was conducted utilizing only the A1163 reference strain, so it is unclear as of yet how generalizable our results will be to other, naturally-occurring isolates. Future studies should employ different clinical and environmental strains to determine the generalizability of aneuploidy in *A. fumigatus*. A recent study, which identified multiple independent segmental duplications in azole-resistant clinical isolates[16], supports the hypothesis that genome instability is generalizable in *A. fumigatus*, although the frequency at which these events occur relative to other modes of acquired resistance, and whether strain-specific variables influence the propensity to become aneuploid, is not yet known.

This study on the effects of aneuploidy on responses to distinct antimicrobial compounds lays a foundation for future inquiry into how flexible genomic changes can drive beneficial stress responses and increase the odds of survival in response to both ecological competition and clinical antimicrobial compounds. Given the large number of genes undergoing copy number changes in aneuploids, it is likely that aneuploidy could also confer advantages in other infection-relevant stressful situations. During host infection, *A. fumigatus* encounters a diverse range of stresses including temperature shifts, changes in pH and oxygen tension, and immune responses such as reactive oxygen species and phagocytosis. Success as a pathogen therefore requires an ability to rapidly adapt to varied and often combinatorial stresses. Investigating how genomic plasticity may

influence this organism's adaptive capacity offers the potential to expand our understanding of its ability to cause human disease and to persist in highly variable environments.

## Resource Availability

*Lead contact*

Requests for resources and further information should be directed to, and will be fulfilled by, the lead contact, Joseph Heitman (heitm001@duke.edu).

*Materials availability*

All unique materials generated in this study are available without restriction from the lead contact.

*Data and code availability*

All raw DNA- and RNA-seq data are deposited at NCBI under Bioproject PRJNA1335234 and PRJNA1335235. Processed sequencing data (variant calls and DESeq results) are included in the Supplemental Material. All original code generated for this project is available at: https://github.com/annalehmann/Afum_FK506_resistance and https://github.com/annalehmann/Afum_Chr7_aneuploids.

## Acknowledgments

We thank the Duke University Sequencing and Genomic Technologies Core Facility for performing the sequencing and Dr. Paul Magwene, Dr. Adrianna San Roman, Dr. Marco Coelho, Dr. Vikas Yadav, and Anna Mackey for assistance and advice with analyzing the DNA- and RNA-sequencing data. We also thank Dr. Robert Cramer for providing the *A. fumigatus* strains and selectable marker plasmids, Dr. Joe Vasselli for sharing a custom 3D-printed microscopy growth chamber, and the members of the Heitman Lab and the Duke mycology community for constructive discussion throughout this project. This study was supported by the NIH/NIAID grants 5R01AI172451-03 and 5R01AI170543-04 (JH) and NIH/NIGMS 1R35GM156119 (NPK). JH is also co-director and fellow of the Canadian Institute for Advanced Research (CIFAR) program Fungal Kingdom: Threats and Opportunities.

## Author Contributions

Conceptualization: A.E.L. and J.H.; Investigation: A.E.L. and E.A.R.; Data analysis: A.E.L. and E.A.R.; Writing – original draft: A.E.L. and E.A.R.; Writing – review & editing: J.H. and N.P.K.; Funding acquisition: J.H. and N.P.K.

## Declaration of Interests

The authors declare no competing interests.

**Supplemental Information**

Document S1: Figures S1-S5; Table S4.

Table S1. High- and medium-impact coding region variants in all FK506-resistant isolates.

Table S2. Gene expression changes in Chr7 aneuploids +/- FK506.

Table S3. Sequence variants between our A1163 laboratory strain and the published reference genome.

**Materials and Methods**

*Strains and growth conditions*

The A1163 reference strain served as the euploid wild type throughout this study. Strains were cultured on 1.5% agar Aspergillus Minimal Medium (AMM), which was prepared as described by Hill and Kafer[90]. All FK506 experiments on agar plates and in liquid culture were performed in AMM with FK506 at a concentration of 1 µg/mL. Conidia were grown for experiments on AMM or AMM+FK506 for 3 days at 37°C. Unstable aneuploids were maintained on +FK506 plates to ensure retention of the ploidy differences. Conidia were collected from plates by flooding the surface of the plate with 0.01% Tween 80, manually dislodging conidia with a cell scraper, and filtering through Miracloth (Millipore Sigma). Conidia were counted with a hemacytometer.

*DNA extraction and sequencing*

Biomass for DNA extraction was obtained by inoculating 5 mL AMM or AMM+FK506 with conidia at a density of $5x10^5$ conidia/mL and incubating at 37°C rotating at 70 rpm on a roller drum for 16-24 hours. Biomass was collected and washed 1x with $diH_2O$, then frozen at -80°C for >1 hour and lyophilized until dry. DNA was extracted following a modified MasterPure (Biosearch Technologies) procedure. First, lyophilized tissue was bead-beaten with 2 mm glass beads for 1 minute. The remainder of the procedure was carried out according to the manufacturer's instructions. Nucleic acid pellets were resuspended in nuclease-free water and quality was assessed by gel electrophoresis. DNA concentration was quantified with a Qubit fluorometer using the DNA broad-range kit (Thermo Fisher Scientific).

DNA sequencing was carried out by the Duke University Sequencing and Genomic Technologies Core Facility. Libraries were prepared using the Kapa HyperPrep kit (Kapa Bioscience). Pooled libraries were sequenced on an Illumina Novaseq X Plus instrument in 150 bp paired-end reads.

*DNA-seq data analysis*

For sequence variant identification, DNA-seq reads were aligned to the A1163 reference genome[56] with snippy[91], using the default parameters. Resulting vcf files served as input for snpEff[92], which compares variants to a preconfigured A1163 database and predicts variant effects on the coding transcript (low, medium, or high). For the resistant isolates, variants in coding regions only were identified with the flags –no-downstream, –no-upstream, and –no-intergenic. Unique variants were determined by filtering out any that were shared with our laboratory A1163 parental strain (Table S3).

Ploidy was determined by comparing coverage depth along 500 bp windows to genome-wide normalized read depth. Reads were aligned to the chromosome-level CEA10 reference assembly[93] with minimap2[94], using settings for paired-end short reads. Aligned reads were filtered by a threshold of q30 with samtools[95]. Mosdepth[96] was used to calculate read depth over 500 bp windows. The resulting bed files were analyzed in R to compare depth in each window to genome-wide normalized coverage. Data were visualized with ggplot2[97].

*Phenotypic assays*

*FK506 spot growth and imaging*

$10^5$ conidia were spotted on AMM + 1 µg/mL FK506 and incubated at 37°C for 2 days. Images of hyphal growth at the colony edge were acquired with an AxioScop 2 fluorescence microscope with 4x objective (Zeiss). Experiments were performed in at least 3 biologically independent replicates.

*Imaging of submerged hyphal growth*

100µL conidia at a concentration of $10^3$ conidia/mL in AMM ± 1 µg/mL FK506 were inoculated in a custom 3D-printed growth chamber[98] encased between 2 transparent slides. Growth chambers were incubated at 37°C for 24 hours. Hyphal growth images were acquired on an AxioScop 2 fluorescence microscope with 10x and 20x objectives (Zeiss). Experiments were performed in biological triplicate.

*Transcriptomics*

*RNA extraction and sequencing*

Biomass for RNA extraction was obtained from $10^6$ conidia/mL cultures in 25 mL AMM or AMM+FK506 grown for 16 hours at 37° with shaking at 200 RPM. Biomass was harvested, washed 1x with sterile di$H_2O$, frozen at -80°C for >1 hour, and lyophilized until dry. Lyophilized tissue was bead-beaten for 1 minute with 2 mm glass beads and RNA was extracted with the Qiagen RNeasy Plant Mini Kit according to the manufacturer's instructions (Qiagen). RNA concentration was measured a Qubit fluorometer using the RNA broad-range kit (Thermo Fisher Scientific).

RNA was sequenced by the Duke University Sequencing and Genomic Technologies Core Facility. Poly-A enriched libraries were prepared from samples with RIN ≥ 7 using the Kapa mRNA-seq HyperPrep kit (Kapa Bioscience). Pooled libraries were sequenced on an Illumina Novaseq X Plus instrument in 150 bp paired-end reads.

*RNA-seq data analysis*

Illumina universal adaptors were trimmed from paired reads with CutAdapt (v4.9). Trimmed reads were then aligned to the A1163 reference assembly[56] with HISAT2 (v2.2.1)[99]. Counts per gene were quantified with featureCounts (v2.0.6)[100]. Exploratory data analysis and differential expression analysis were performed with DESeq2 (v1.44.0)[101]. Prior to analysis, transcript counts were normalized by transcripts per million (TPM) within each replicate and genes with at least 1 TPM in 1 sample were retained. Clustering and principal component analyses were performed using vst normalized values for the top 1000 most variable genes generated by DESeq2. Differential expression analysis was carried out in DESeq2 with alpha = 0.05 and a $\log_2$FC cutoff of +/- 1 was applied to identify DEGs from the resulting expression data. The R packages EnhancedVolcano (v1.22.0) (https://github.com/kevinblighe/EnhancedVolcano) and pheatmap (v1.0.13) (https://github.com/raivokolde/pheatmap) were used for data visualization.

nscR *overexpression strain construction*

The *nscR*$^{OE}$ strain was generated in the A1163 background by ectopic integration of *nscR* (AFUB_086680) driven by an *A. fumigatus gpdA* promoter amplified from the Af293 reference strain (Fungal Genetics Stock Center A1100). The *gpdA* promoter ($_p$*gpdA*) was selected as the 996 bp immediately upstream of the *gpdA* (Afu5g01970) open reading frame using primers AEL68 and AEL69. The promoter was fused to the *nscR* open reading frame and the 504 bases immediately 3' of the stop codon, which was amplified from A1163 gDNA with primers AEL70 and AEL71, and the hygromycin resistance marker *hygR*. The $_p$*gpdA*$^{AF}$*-nscR* overexpression construct fused to *hygR* selectable marker was amplified with primers AEL75 and AEL76. The resulting product was used to transform A1163 protoplasts as described previously[102,103]. Transformants were selected on osmotically-stabilized minimal medium (AMM + 1.2 M sorbitol) containing hygromycin. Successful transformants were single spored, and genomic integration of the construct was verified by PCR and expression was measured by RT-qPCR as described below, with RNA obtained from WT and *nscR*$^{OE}$ under the same conditions ± FK506 used for RNA-seq. All primer sequences used are listed in Table S4.

*Reverse transcriptase quantitative PCR (RT-qPCR)*

2.5 to 5 µg of RNA was DNase treated using the TURBO DNA-free kit (Invitrogen) following the manufacturer's instructions. Post-DNase treatment RNA integrity was verified by running a sample of the RNA on an agarose gel. cDNA synthesis was carried out using 500 ng of DNase-treated RNA as described previously[104]. RT-qPCR was run on a QuantStudio 3 or QuantStudio 6 Pro system (Thermo Fisher Scientific). Gene expression was normalized to *actA* and *tubA* in all experiments. Fold change values were calculated by the $2^{-\Delta\Delta Ct}$ method[105].

*Metabolomic studies*

Four biological replicates of each strain were cultured at $10^6$ conidia/mL in 25 mL of GMM medium supplemented with 1 µg FK506/mL and incubated for two days at 37 °C with shaking at 200 rpm. After the fermentation period, each fungal culture and four medium replicates (considered as blanks) were extracted by maceration with 25 mL of EtOAc/MeOH/AcOH (89:10:1) overnight, with shaking at 120 rpm. The organic phase was then separated and evaporated to dryness under reduced pressure. The resulting organic extracts were dissolved in MeOH at a concentration of 50 mg/mL, and serial dilutions (1:10 and 1:50) were prepared to obtain solutions at 0.1 mg/mL for LC-MS analysis. Then, a 5 µL aliquot of each sample was analyzed by UPLC coupled to an Orbitrap Exploris™ 240 mass spectrometer, acquiring both $MS^1$ and MS/MS spectra, using an Acquity BEH-C18 column (2.1 mm × 100 mm, 1.7 µm).

The chromatographic method consisted of a one minute isocratic elution of 10% MeCN in $H_2O$ containing 0.05% formic acid, followed by a linear gradient from 10% to 100% MeCN over 20 minutes, and a 2.5-minute wash with 100% MeCN. The flow rate was maintained at 0.3 mL/min throughout the run, with alternating positive and negative ion detection over an *m*/*z* range of 120–1500 for MS/MS acquisition. Precursor ions were fragmented using higher-energy collisional dissociation (HCD) with dynamic exclusion set to 3 s.

Once the LC-MS/MS data were acquired, the raw files generated from these analyses were converted to .mzML format using MSConvert[106], applying the peak-picking filter for both $MS^1$ and $MS^2$. Spectra were processed in MZmine (v4.7.8)[107]. Mass detection was performed using the lowest signal factor, with a noise threshold set at 5.0 for $MS^1$ and 2.5 for $MS^2$. A chromatogram was constructed using the Chromatogram Builder algorithm in positive polarity mode, with parameters set to a minimum of 4 consecutive scans, a minimum intensity of $1\times10^4$ for consecutive scans, a minimum absolute height of $5\times10^4$, and a mass tolerance of 10 ppm.

The resulting chromatogram features were then processed using Savitzky-Golay smoothing (5 scans retention time width), the Local Minimum Feature Resolver, a 13C isotope filter, the Join Aligner, Feature Finder, and duplicate peak filter. From this processed feature list, features detected in the blank replicates were manually removed, yielding a total of 4,495 features. This curated feature list was used for principal component analysis (PCA) with Pareto scaling and missing value

imputation (set at 1/5 of the minimum value), for pairwise comparisons using unpaired Volcano Plots, and for molecular network construction following the Feature-based Molecular Networking workflow with default parameters[108].

The abundance of secondary metabolites was represented using the area under the curve of the target feature (included in chromatograms, bar graphs, and heatmaps), based on LC-MS data acquired in either negative or positive ionization mode. PCA plots, Volcano Plots, chromatograms, bar graphs, and heatmaps were generated with Prism 10.6.0. The molecular network was visualized using Cytoscape (v3.10.3)[109]. The identities of fumitremorgin C, fumagillin, pyripyropene A, fumiquinazoline F, and FK506 were confirmed by comparison of their chromatographic and spectrometric data with authentic standards. The identity of pseurotin A was supported by matching the fragmentation spectrum of the detected molecular ion to a high-quality gold-standard reference deposited in the GNPS database (https://gnps.ucsd.edu/ProteoSAFe/gnpslibraryspectrum.jsp?SpectrumID=CCMSLIB00011906568#%7B%7D). The ergosterol-type triterpenoids class was supported by the predicted formula and by the comparison of the fragmentation pattern with those reported by Lucie Ory et al[110].

*Antifungal susceptibility tests*

Susceptibility to voriconazole, isavuconazole, and posaconazole was tested using commercially-available E-test strips (Liofilchem, Waltham, MA, USA). As described previously[111], 5 mL of AMM agar containing $10^5$ conidia was overlaid on an AMM plate and allowed to solidify, then an E-test strip was placed in the center of the plate. E-test plates were incubated at 37°C in the dark for 3 days. MICs were observed at 2 and 3 days to account for the slower growth rate of aneuploids relative to euploid. MICs after 3 days are reported for all strains.

Broth dilution MIC assays were performed in both AMM and RPMI broth according to the established standard CLSI procedure[112]. MIC values are reported after 2 days incubation at 37°C. All reported MIC values are averages of biological triplicates.

**References**


1. Knouse, K.A., Davoli, T., Elledge, S.J., and Amon, A. (2017). Aneuploidy in cancer: seq-ing answers to old questions. Annu. Rev. Cancer Biol. *1*, 335–354. https://doi.org/10.1146/annurev-cancerbio-042616-072231.
2. Ben-David, U., and Amon, A. (2020). Context is everything: aneuploidy in cancer. Nat. Rev. Genet. *21*, 44–62. https://doi.org/10.1038/s41576-019-0171-x.
3. Torres, E.M., Williams, B.R., and Amon, A. (2008). Aneuploidy: cells losing their balance. Genetics *179*, 737–746. https://doi.org/10.1534/genetics.108.090878.

4. Gilchrist, C., and Stelkens, R. (2019). Aneuploidy in yeast: segregation error or adaptation mechanism? Yeast *36*, 525–539. https://doi.org/10.1002/yea.3427.
5. Sheltzer, J.M., Blank, H.M., Pfau, S.J., Tange, Y., George, B.M., Humpton, T.J., Brito, I.L., Hiraoka, Y., Niwa, O., and Amon, A. (2011). Aneuploidy drives genomic instability in yeast. Science *333*, 1026–1030. https://doi.org/10.1126/science.1206412.
6. Sunshine, A.B., Payen, C., Ong, G.T., Liachko, I., Tan, K.M., and Dunham, M.J. (2015). The fitness consequences of aneuploidy are driven by condition-dependent gene effects. PLOS Biol. *13*, e1002155. https://doi.org/10.1371/journal.pbio.1002155.
7. Yona, A.H., Manor, Y.S., Herbst, R.H., Romano, G.H., Mitchell, A., Kupiec, M., Pilpel, Y., and Dahan, O. (2012). Chromosomal duplication is a transient evolutionary solution to stress. Proceed. Nat. Acad. Sci. USA *109*, 21010–21015. https://doi.org/10.1073/pnas.1211150109.
8. Gresham, D., Desai, M.M., Tucker, C.M., Jenq, H.T., Pai, D.A., Ward, A., DeSevo, C.G., Botstein, D., and Dunham, M.J. (2008). The repertoire and dynamics of evolutionary adaptations to controlled nutrient-limited environments in yeast. PLOS Genet. *4*, e1000303. https://doi.org/10.1371/journal.pgen.1000303.
9. Todd, R.T., Forche, A., and Selmecki, A. (2017). Ploidy variation in fungi: polyploidy, aneuploidy, and genome evolution. Microbiology Spectrum *5*, 10.1128/microbiolspec.funk-0051–2016. https://doi.org/10.1128/microbiolspec.funk-0051-2016.
10. Selmecki, A., Forche, A., and Berman, J. (2006). Aneuploidy and isochromosome formation in drug-resistant Candida albicans. Science *313*, 367–370. https://doi.org/10.1126/science.1128242.
11. Sun, L., Li, H., Yan, T., Fang, T., Wu, H., Cao, Y., Lu, H., Jiang, Y., and Yang, F. (2023). Aneuploidy mediates rapid adaptation to a subinhibitory amount of fluconazole in Candida albicans. Microbiol. Spectr. *11*, e03016-22. https://doi.org/10.1128/spectrum.03016-22.
12. Perepnikhatka, V., Fischer, F.J., Niimi, M., Baker, R.A., Cannon, R.D., Wang, Y.-K., Sherman, F., and Rustchenko, E. (1999). Specific chromosome alterations in fluconazole-resistant mutants of Candida albicans. J. of Bacteriol. *181*, 4041–4049. https://doi.org/10.1128/jb.181.13.4041-4049.1999.
13. Yang, F., Gritsenko, V., Lu, H., Zhen, C., Gao, L., Berman, J., and Jiang, Y. (2021). Adaptation to fluconazole via aneuploidy enables cross-adaptation to Amphotericin B and Flucytosine in Cryptococcus neoformans. Microbiol. Spectr. *9*, e00723-21. https://doi.org/10.1128/Spectrum.00723-21.
14. Zhang, Z., Sun, L., Fu, B., Deng, J., Jia, C., Miao, M., Yang, F., Cao, Y., and Yan, T. (2024). Aneuploidy underlies brefeldin A-induced antifungal drug resistance in Cryptococcus neoformans. Front. Cell. Infect. Microbiol. *14*. https://doi.org/10.3389/fcimb.2024.1397724.

15. Barda, O., Sadhasivam, S., Gong, D., Doron-Faigenboim, A., Zakin, V., Drott, M.T., and Sionov, E. (2023). Aneuploidy formation in the filamentous fungus Aspergillus flavus in response to azole stress. Microbiol. Spectr. *11*, e04339-22. https://doi.org/10.1128/spectrum.04339-22.
16. Khateb, A., Gago, S., Bromley, M., Richardson, M., and Bowyer, P. (2023). Aneuploidy Is associated with azole resistance in Aspergillus fumigatus. Antimicrob. Agents Chemother. *67*, e01253-22. https://doi.org/10.1128/aac.01253-22.
17. Denning, D.W. Global incidence and mortality of severe fungal disease. Lancet Infect. Dis. *24*, 428–438. https://doi.org/10.1016/S1473-3099(23)00692-8.
18. Nguyen, K.-H., Chollet-Krugler, M., Gouault, N., and Tomasi, S. (2013). UV-protectant metabolites from lichens and their symbiotic partners. Nat. Prod. Rep. *30*, 1490–1508. https://doi.org/10.1039/C3NP70064J.
19. Brakhage, A.A., and Liebmann, B. (2005). Aspergillus fumigatus conidial pigment and cAMP signal transduction: significance for virulence. Med. Mycol. *43 Suppl 1*, S75-82. https://doi.org/10.1080/13693780400028967.
20. Berkova, N., Lair-Fulleringer, S., Féménia, F., Huet, D., Wagner, M.-C., Gorna, K., Tournier, F., Ibrahim-Granet, O., Guillot, J., Chermette, R., et al. (2006). Aspergillus fumigatus conidia inhibit tumour necrosis factor- or staurosporine-induced apoptosis in epithelial cells. Int. Immunol. *18*, 139–150. https://doi.org/10.1093/intimm/dxh356.
21. Gardiner, D.M., Waring, P., and Howlett, B.J. (2005). The epipolythiodioxopiperazine (ETP) class of fungal toxins: distribution, mode of action, functions and biosynthesis. Microbiology *151*, 1021–1032. https://doi.org/10.1099/mic.0.27847-0.
22. Bok, J.W., Chung, D., Balajee, S.A., Marr, K.A., Andes, D., Nielsen, K.F., Frisvad, J.C., Kirby, K.A., and Keller, N.P. (2006). GliZ, a Transcriptional Regulator of Gliotoxin Biosynthesis, Contributes to Aspergillus fumigatus Virulence. Infect. Immun. *74*, 6761–6768. https://doi.org/10.1128/iai.00780-06.
23. Pardo, J., Urban, C., Galvez, E.M., Ekert, P.G., Müller, U., Kwon-Chung, J., Lobigs, M., Müllbacher, A., Wallich, R., Borner, C., et al. (2006). The mitochondrial protein Bak is pivotal for gliotoxin-induced apoptosis and a critical host factor of Aspergillus fumigatus virulence in mice. J. Cell Biol. *174*, 509–519. https://doi.org/10.1083/jcb.200604044.
24. Spikes, S., Xu, R., Nguyen, C.K., Chamilos, G., Kontoyiannis, D.P., Jacobson, R.H., Ejzykowicz, D.E., Chiang, L.Y., Filler, S.G., and May, G.S. (2008). Gliotoxin production in Aspergillus fumigatus contributes to host-specific differences in virulence. J. Infect. Dis. *197*, 479–486. https://doi.org/10.1086/525044.
25. Cramer, R.A., Rivera, A., and Hohl, T.M. (2011). Immune responses against Aspergillus fumigatus: what have we learned? Curr. Opin. Infect. Dis. *24*, 315–322. https://doi.org/10.1097/QCO.0b013e328348b159.

26. Raffa, N., and Keller, N.P. (2019). A call to arms: Mustering secondary metabolites for success and survival of an opportunistic pathogen. PLOS Pathog. *15*, e1007606. https://doi.org/10.1371/journal.ppat.1007606.
27. Lim, F.Y., Sanchez, J.F., Wang, C.C.C., and Keller, N.P. (2012). Chapter fifteen - toward awakening cryptic secondary metabolite gene clusters in filamentous fungi. Methods in Enzymology Natural Product Biosynthesis by Microorganisms and Plants, Part C., D. A. Hopwood, ed. (Academic Press), pp. 303–324. https://doi.org/10.1016/B978-0-12-404634-4.00015-2.
28. O'Hanlon, K.A., Cairns, T., Stack, D., Schrettl, M., Bignell, E.M., Kavanagh, K., Miggin, S.M., O'Keeffe, G., Larsen, T.O., and Doyle, S. (2011). Targeted disruption of nonribosomal peptide synthetase pes3 augments the virulence of Aspergillus fumigatus. Infect. Immun. *79*, 3978–3992. https://doi.org/10.1128/iai.00192-11.
29. Yin, W.-B., Baccile, J.A., Bok, J.W., Chen, Y., Keller, N.P., and Schroeder, F.C. (2013). A nonribosomal peptide synthetase-derived iron(III) complex from the pathogenic fungus Aspergillus fumigatus. J. Am. Chem. Soc. *135*, 2064–2067. https://doi.org/10.1021/ja311145n.
30. Tsunematsu, Y., Ishikawa, N., Wakana, D., Goda, Y., Noguchi, H., Moriya, H., Hotta, K., and Watanabe, K. (2013). Distinct mechanisms for spiro-carbon formation reveal biosynthetic pathway crosstalk. Nat. Chem. Biol. *9*, 818–825. https://doi.org/10.1038/nchembio.1366.
31. O'Keeffe, G., Hammel, S., Owens, R.A., Keane, T.M., Fitzpatrick, D.A., Jones, G.W., and Doyle, S. (2014). RNA-seq reveals the pan-transcriptomic impact of attenuating the gliotoxin self-protection mechanism in Aspergillus fumigatus. BMC Genomics *15*, 894. https://doi.org/10.1186/1471-2164-15-894.
32. Krespach, M.K.C., Stroe, M.C., Netzker, T., Rosin, M., Zehner, L.M., Komor, A.J., Beilmann, J.M., Krüger, T., Scherlach, K., Kniemeyer, O., et al. (2023). Streptomyces polyketides mediate bacteria–fungi interactions across soil environments. Nat. Microbiol. *8*, 1348–1361. https://doi.org/10.1038/s41564-023-01382-2.
33. König, C.C., Scherlach, K., Schroeckh, V., Horn, F., Nietzsche, S., Brakhage, A.A., and Hertweck, C. (2013). Bacterium induces cryptic meroterpenoid pathway in the pathogenic fungus Aspergillus fumigatus. ChemBioChem *14*, 938–942. https://doi.org/10.1002/cbic.201300070.
34. Nützman, H.-W., Reyes-Dominguez, Y., Scherlach, K., Schroeckh, V., Horn, F., Gacek, A., Schümann, J., Hertwerk, C., Strauss, J., and Brakhage, A.A. (2011). Bacteria-induced natural product formation in the fungus Aspergillus nidulans requires Saga/Ada-mediated histone acetylation. Proceed. Nat. Acad. Sci. USA *108*, 14282–14287. https://doi.org/10.1073/pnas.1103523108.

35. Zuck, K.M., Shipley, S., and Newman, D.J. (2011). Induced production of N-formyl alkaloids from Aspergillus fumigatus by co-culture with Streptomyces peucetius. J. Nat. Prod. *74*, 1653–1657. https://doi.org/10.1021/np200255f.
36. Stroe, M.C., Netzker, T., Scherlach, K., Krüger, T., Valiante, V., and Brakhage, A.A. (2020). Targeted induction of a silent fungal gene cluster encoding the bacteria-specific germination inhibitor fumigermin. eLife *9*, e52541. https://doi.org/10.7554/eLife.52541.
37. Schroeckh, V., Scherlach, K., Nützmann, H.-W., Shelest, E., Schmidt-Heck, W., Schuemann, J., Martin, K., Hertweck, C., and Brakhage, A.A. (2009). Intimate bacterial–fungal interaction triggers biosynthesis of archetypal polyketides in Aspergillus nidulans. Proceed. Nat. Acad. Sci. USA *106*, 14558–14563. https://doi.org/10.1073/pnas.0901870106.
38. Losada, L., Ajayi, O., Frisvad, J.C., Yu, J., and Nierman, W.C. (2009). Effect of competition on the production and activity of secondary metabolites in Aspergillus species. Med. Mycol. *47*, S88–S96. https://doi.org/10.1080/13693780802409542.
39. Calo, S., Nicolás, F.E., Lee, S.C., Vila, A., Cervantes, M., Torres-Martinez, S., Ruiz-Vazquez, R.M., Cardenas, M.E., and Heitman, J. (2017). A non-canonical RNA degradation pathway suppresses RNAi-dependent epimutations in the human fungal pathogen Mucor circinelloides. PLOS Genet. *13*, e1006686. https://doi.org/10.1371/journal.pgen.1006686.
40. Calo, S., Shertz-Wall, C., Lee, S.C., Bastidas, R.J., Nicolás, F.E., Granek, J.A., Mieczkowski, P., Torres-Martínez, S., Ruiz-Vázquez, R.M., Cardenas, M.E., et al. (2014). Antifungal drug resistance evoked via RNAi-dependent epimutations. Nature *513*, 555–558. https://doi.org/10.1038/nature13575.
41. Priest, S.J., Yadav, V., Roth, C., Dahlmann, T.A., Kück, U., Magwene, P.M., and Heitman, J. (2022). Uncontrolled transposition following RNAi loss causes hypermutation and antifungal drug resistance in clinical isolates of Cryptococcus neoformans. Nat. Microbiol. *7*, 1239–1251. https://doi.org/10.1038/s41564-022-01183-z.
42. Yadav, V., Averette, A.F., Upadhya, R., and Heitman, J. (2025). Calcineurin controls the cytokinesis machinery during thermal stress in Cryptococcus deneoformans. Proceed. Nat. Acad. Sci. USA *122*, e2503751122. https://doi.org/10.1073/pnas.2503751122.
43. Huang, J., Larmore, C.J., Priest, S.J., Xu, Z., Dietrich, F.S., Yadav, V., Magwene, P.M., Sun, S., and Heitman, J. (2024). Distinct evolutionary trajectories following loss of RNA interference in *Cryptococcus neoformans*. Proceed. Nat. Acad. Sci. USA *121*, e2416656121. https://doi.org/10.1073/pnas.2416656121.
44. Liu, J., Farmer, J.D., Lane, W.S., Friedman, J., Weissman, I., and Schreiber, S.L. (1991). Calcineurin is a common target of cyclophilin-cyclosporin A and FKBP-FK506 complexes. Cell *66*, 807–815. https://doi.org/10.1016/0092-8674(91)90124-H.

45. Ho, S., Clipstone, N., Timmermann, L., Northrop, J., Graef, I., Fiorentino, D., Nourse, J., and Crabtree, G.R. (1996). The mechanism of action of cyclosporin A and FK506. Clin. Immunol. Immunopathol. *80*, S40–S45. https://doi.org/10.1006/clin.1996.0140.
46. Hemenway, C.S., and Heitman, J. (1999). Calcineurin. Cell Biochem. Biophys. *30*, 115–151. https://doi.org/10.1007/BF02737887.
47. Lee, S.C., Li, A., Calo, S., and Heitman, J. (2013). Calcineurin plays key roles in the dimorphic transition and virulence of the human pathogenic zygomycete Mucor circinelloides. PLOS Pathog. *9*, e1003625. https://doi.org/10.1371/journal.ppat.1003625.
48. Juvvadi, P.R., Fortwendel, J.R., Pinchai, N., Perfect, B.Z., Heitman, J., and Steinbach, W.J. (2008). Calcineurin localizes to the hyphal septum in Aspergillus fumigatus: implications for septum formation and conidiophore development. Eukaryot. Cell *7*, 1606–1610. https://doi.org/10.1128/ec.00200-08.
49. Steinbach, W.J., Cramer, R.A., Perfect, B.Z., Asfaw, Y.G., Sauer, T.C., Najvar, L.K., Kirkpatrick, W.R., Patterson, T.F., Benjamin, D.K., Heitman, J., et al. (2006). Calcineurin controls growth, morphology, and pathogenicity in Aspergillus fumigatus. Eukaryot. Cell *5*, 1091–1103. https://doi.org/10.1128/ec.00139-06.
50. Cramer, R.A., Perfect, B.Z., Pinchai, N., Park, S., Perlin, D.S., Asfaw, Y.G., Heitman, J., Perfect, J.R., and Steinbach, W.J. (2008). Calcineurin target CrzA regulates conidial germination, hyphal growth, and pathogenesis of Aspergillus fumigatus. Eukaryot. Cell *7*, 1085–1097. https://doi.org/10.1128/ec.00086-08.
51. Juvvadi, P.R., Fortwendel, J.R., Rogg, L.E., Burns, K.A., Randell, S.H., and Steinbach, W.J. (2011). Localization and activity of the calcineurin catalytic and regulatory subunit complex at the septum is essential for hyphal elongation and proper septation in Aspergillus fumigatus. Mol. Microbiol. *82*, 1235–1259. https://doi.org/10.1111/j.1365-2958.2011.07886.x.
52. Steinbach, W.J., Schell, W.A., Blankenship, J.R., Onyewu, C., Heitman, J., and Perfect, J.R. (2004). In vitro interactions between antifungals and immunosuppressants against Aspergillus fumigatus. Antimicrob. Agents Chemother. *48*, 1664–1669. https://doi.org/10.1128/aac.48.5.1664-1669.2004.
53. Falloon, K., Juvvadi, P.R., Richards, A.D., Vargas-Muñiz, J.M., Renshaw, H., and Steinbach, W.J. (2015). Characterization of the FKBP12-encoding genes in Aspergillus fumigatus. PLOS ONE *10*, e0137869. https://doi.org/10.1371/journal.pone.0137869.
54. Juvvadi, P.R., Lamoth, F., and Steinbach, W.J. (2014). Calcineurin as a multifunctional regulator: Unraveling novel functions in fungal stress responses, hyphal growth, drug resistance, and pathogenesis. Fungal Biol. Rev. *28*, 56–69. https://doi.org/10.1016/j.fbr.2014.02.004.

55. Juvvadi, P.R., and Steinbach, W.J. (2015). Calcineurin orchestrates hyphal growth, septation, drug resistance and pathogenesis of Aspergillus fumigatus: where do we go from here? Pathogens *4*, 883–893. https://doi.org/10.3390/pathogens4040883.
56. Fedorova, N.D., Khaldi, N., Joardar, V.S., Maiti, R., Amedeo, P., Anderson, M.J., Crabtree, J., Silva, J.C., Badger, J.H., Albarraq, A., et al. (2008). Genomic islands in the pathogenic filamentous fungus Aspergillus fumigatus. PLOS Genet. *4*, e1000046. https://doi.org/10.1371/journal.pgen.1000046.
57. Chooi, Y.-H., Fang, J., Liu, H., Filler, S.G., Wang, P., and Tang, Y. (2013). Genome mining of a prenylated and immunosuppressive polyketide from pathogenic fungi. Org. Lett. *15*, 780–783. https://doi.org/10.1021/ol303435y.
58. Brakhage, A.A., and Schroeckh, V. (2011). Fungal secondary metabolites – strategies to activate silent gene clusters. Fungal Genet. Biol. *48*, 15–22. https://doi.org/10.1016/j.fgb.2010.04.004.
59. Bok, J.W., and Keller, N.P. (2004). LaeA, a regulator of secondary metabolism in Aspergillus spp. Eukaryot. Cell *3*, 527–535. https://doi.org/10.1128/ec.3.2.527-535.2004.
60. Mózsik, L., Iacovelli, R., Bovenberg, R.A.L., and Driessen, A.J.M. (2022). Transcriptional activation of biosynthetic gene clusters in filamentous fungi. Front. Bioeng. Biotechnol. *10*. https://doi.org/10.3389/fbioe.2022.901037.
61. Seo, H.-W., Wassano, N.S., Amir Rawa, M.S., Nickles, G.R., Damasio, A., and Keller, N.P. (2024). A timeline of biosynthetic gene cluster discovery in Aspergillus fumigatus: from characterization to future perspectives. J. Fungi *10*, 266. https://doi.org/10.3390/jof10040266.
62. Verweij, P.E., Mellado, E., and Melchers, W.J.G. (2007). Multiple-triazole–resistant aspergillosis. N. Engl. J. Med. *356*, 1481–1483. https://doi.org/10.1056/NEJMc061720.
63. Hurst, S.F., Berkow, E.L., Stevenson, K.L., Litvintseva, A.P., and Lockhart, S.R. (2017). Isolation of azole-resistant Aspergillus fumigatus from the environment in the south-eastern USA. J. Antimicrob. Chemother. *72*, 2443–2446. https://doi.org/10.1093/jac/dkx168.
64. Howard, S.J., Cerar, D., Anderson, M.J., Albarrag, A., Fisher, M.C., Pasqualotto, A.C., Laverdiere, M., Arendrup, M.C., Perlin, D.S., and Denning, D.W. (2009). Frequency and evolution of azole resistance in Aspergillus fumigatus associated with treatment failure. Emerg. Infect. Dis. *15*, 1068-1076. https://doi.org/10.3201/eid1507.090043.
65. Snelders, E., Huis in ’t Veld, R.A.G., Rijs, A.J.M.M., Kema, G.H.J., Melchers, W.J.G., and Verweij, P.E. (2009). Possible environmental origin of resistance of Aspergillus fumigatus to medical triazoles. Appl. Environ. Microbiol. *75*, 4053–4057. https://doi.org/10.1128/AEM.00231-09.
66. Snelders, E., Van Der Lee, H.A.L., Kuijpers, J., Rijs, A.J.M.M., Varga, J., Samson, R.A., Mellado, E., Donders, A.R.T., Melchers, W.J.G., and Verweij, P.E. (2008). Emergence of azole resistance

in Aspergillus fumigatus and spread of a single resistance mechanism. PLoS Med. *5*, e219. https://doi.org/10.1371/journal.pmed.0050219.

67. Alvarez-Moreno, C., Lavergne, R.-A., Hagen, F., Morio, F., Meis, J.F., and Le Pape, P. (2017). Azole-resistant Aspergillus fumigatus harboring TR34/L98H, TR46/Y121F/T289A and TR53 mutations related to flower fields in Colombia. Sci. Rep. *7*, 45631. https://doi.org/10.1038/srep45631.

68. Mellado, E., Garcia-Effron, G., Alcázar-Fuoli, L., Melchers, W.J.G., Verweij, P.E., Cuenca-Estrella, M., and Rodríguez-Tudela, J.L. (2007). A new Aspergillus fumigatus resistance mechanism conferring in vitro cross-resistance to azole antifungals involves a combination of cyp51A alterations. Antimicrob. Agents Chemother. *51*, 1897–1904. https://doi.org/10.1128/aac.01092-06.

69. Buied, A., Moore, C.B., Denning, D.W., and Bowyer, P. (2013). High-level expression of cyp51B in azole-resistant clinical Aspergillus fumigatus isolates. J. Antimicrob. Chemother. *68*, 512–514. https://doi.org/10.1093/jac/dks451.

70. Nywening, A.V., Thorn, H.I., Xie, J., Martin-Vicente, A., Guruceaga, X., Ge, W., Gibbons, J.G., and Fortwendel, J.R. (2025). Loss of the Aspergillus fumigatus spindle assembly checkpoint components, SldA or SldB, generates triazole heteroresistant conidial populations. Microbiol. Spectr. *13*, e00536-25. https://doi.org/10.1128/spectrum.00536-25.

71. Colabardini, A.C., Wang, F., Dong, Z., Pardeshi, L., Rocha, M.C., Costa, J.H., dos Reis, T.F., Brown, A., Jaber, Q.Z., Fridman, M., et al. (2022). Heterogeneity in the transcriptional response of the human pathogen Aspergillus fumigatus to the antifungal agent caspofungin. Genetics *220*, iyab183. https://doi.org/10.1093/genetics/iyab183.

72. Bergmann, S., Funk, A.N., Scherlach, K., Schroeckh, V., Shelest, E., Horn, U., Hertweck, C., and Brakhage, A.A. (2010). Activation of a silent fungal polyketide biosynthesis pathway through regulatory cross talk with a cryptic nonribosomal peptide synthetase gene cluster. Appl. Environ. Microbiol. *76*, 8143–8149. https://doi.org/10.1128/AEM.00683-10.

73. Tannous, J., Kumar, D., Sela, N., Sionov, E., Prusky, D., and Keller, N.P. (2018). Fungal attack and host defence pathways unveiled in near-avirulent interactions of Penicillium expansum creA mutants on apples. Mol. Plant Pathol. *19*, 2635–2650. https://doi.org/10.1111/mpp.12734.

74. Shimizu, K., Hicks, J.K., Huang, T.-P., and Keller, N.P. (2003). Pka, Ras and RGS protein interactions regulate activity of AflR, a Zn(II)2Cys6 transcription factor in Aspergillus nidulans. Genetics *165*, 1095–1104. https://doi.org/10.1093/genetics/165.3.1095.

75. Wiemann, P., Lechner, B.E., Baccile, J.A., Velk, T.A., Yin, W.-B., Bok, J.W., Pakala, S., Losada, L., Nierman, W.C., Schroeder, F.C., et al. (2014). Perturbations in small molecule synthesis uncovers an iron-responsive secondary metabolite network in Aspergillus fumigatus. Front. Microbiol. *5*. https://doi.org/10.3389/fmicb.2014.00530.

76. Wang, W., Drott, M., Greco, C., Luciano-Rosario, D., Wang, P., and Keller, N.P. (2021). Transcription factor repurposing offers insights into evolution of biosynthetic gene cluster regulation. mBio *12*, e0139921. https://doi.org/10.1128/mBio.01399-21.
77. Shostak, K., Bonner, C., Sproule, A., Thapa, I., Shields, S.W.J., Blackwell, B., Vierula, J., Overy, D., and Subramaniam, R. (2020). Activation of biosynthetic gene clusters by the global transcriptional regulator TRI6 in Fusarium graminearum. Mol. Microbiol. *114*, 664–680. https://doi.org/10.1111/mmi.14575.
78. Kong, Q., Chang, P.-K., Li, C., Hu, Z., Zheng, M., Sun, Q., and Shan, S. (2020). Identification of AflR binding sites in the genome of Aspergillus flavus by ChIP-seq. J. Fungi *6*, 52. https://doi.org/10.3390/jof6020052.
79. Ehrlich, K.C., Montalbano, B.G., and Cotty, P.J. (2003). Sequence comparison of *aflR* from different *Aspergillus* species provides evidence for variability in regulation of aflatoxin production. Fungal Genet. Biol. *38*, 63–74. https://doi.org/10.1016/S1087-1845(02)00509-1.
80. Wang, P., Xu, J., Chang, P.-K., Liu, Z., and Kong, Q. (2022). New insights of transcriptional regulator AflR in Aspergillus flavus physiology. Microbiol. Spectr. *10*, e00791-21. https://doi.org/10.1128/spectrum.00791-21.
81. Slutsky, B., Staebell, M., Anderson, J., Risen, L., Pfaller, M., and Soll, D.R. (1987). “White-opaque transition”: a second high-frequency switching system in Candida albicans. J. Bacteriol. *169*, 189–197. https://doi.org/10.1128/jb.169.1.189-197.1987.
82. Bennett, R.J., and Johnson, A.D. (2005). Mating in Candida albicans and the search for a sexual cycle. Annu. Rev. Microbiol. *59*, 233–255. https://doi.org/10.1146/annurev.micro.59.030804.121310.
83. Miller, M.G., and Johnson, A.D. (2002). White-opaque switching in Candida albicans is controlled by mating-type locus homeodomain proteins and allows efficient mating. Cell *110*, 293–302. https://doi.org/10.1016/S0092-8674(02)00837-1.
84. Lan, C.-Y., Newport, G., Murillo, L.A., Jones, T., Scherer, S., Davis, R.W., and Agabian, N. (2002). Metabolic specialization associated with phenotypic switching in *Candida albicans*. Proceed. Nat. Acad. Sci. USA *99*, 14907–14912. https://doi.org/10.1073/pnas.232566499.
85. Zordan, R.E., Miller, M.G., Galgoczy, D.J., Tuch, B.B., and Johnson, A.D. (2007). Interlocking transcriptional feedback loops control white-opaque switching in Candida albicans. PLOS Biol. *5*, e256. https://doi.org/10.1371/journal.pbio.0050256.
86. Huang, G., Wang, H., Chou, S., Nie, X., Chen, J., and Liu, H. (2006). Bistable expression of WOR1, a master regulator of white–opaque switching in Candida albicans. Proceed. Nat. Acad. Sci. USA *103*, 12813–12818. https://doi.org/10.1073/pnas.0605270103.

87. Zordan, R.E., Galgoczy, D.J., and Johnson, A.D. (2006). Epigenetic properties of white–opaque switching in Candida albicans are based on a self-sustaining transcriptional feedback loop. Proceed. Nat. Acad. Sci. USA *103*, 12807–12812. https://doi.org/10.1073/pnas.0605138103.
88. Blosser, S.J., and Cramer, R.A. (2012). SREBP-dependent triazole susceptibility in Aspergillus fumigatus is mediated through direct transcriptional regulation of erg11A (cyp51A). Antimicrob. Agents Chemother. *56*, 248–257. https://doi.org/10.1128/aac.05027-11.
89. Selmecki, A., Gerami-Nejad, M., Paulson, C., Forche, A., and Berman, J. (2008). An isochromosome confers drug resistance in vivo by amplification of two genes, ERG11 and TAC1. Mol. Microbiol. *68*, 624–641. https://doi.org/10.1111/j.1365-2958.2008.06176.x.
90. Hill, T., and Kafer, E. (2001). Improved protocols for Aspergillus minimal medium: trace element and minimal medium salt stock solutions. Fungal Genet. Rep. *48*, 20–21. https://doi.org/10.4148/1941-4765.1173.
91. Seemann, T. (2024). https://github.com/tseemann/snippy.
92. Cingolani, P., Platts, A., Wang, L.L., Coon, M., Nguyen, T., Wang, L., Land, S.J., Lu, X., and Ruden, D.M. (2012). A program for annotating and predicting the effects of single nucleotide polymorphisms, SnpEff: SNPs in the genome of Drosophila melanogaster strain $w^{1118}$□; iso-2; iso-3. Fly *6*, 80–92. https://doi.org/10.4161/fly.19695.
93. Bowyer, P., Currin, A., Delneri, D., and Fraczek, M.G. (2022). Telomere-to-telomere genome sequence of the model mould pathogen Aspergillus fumigatus. Nat. Commun. *13*, 5394. https://doi.org/10.1038/s41467-022-32924-7.
94. Li, H. (2018). Minimap2: pairwise alignment for nucleotide sequences. Bioinformatics *34*, 3094–3100. https://doi.org/10.1093/bioinformatics/bty191.
95. Li, H., Handsaker, B., Wysoker, A., Fennell, T., Ruan, J., Homer, N., Marth, G., Abecasis, G., Durbin, R., and 1000 Genome Project Data Processing Subgroup (2009). The sequence alignment/map format and SAMtools. Bioinformatics *25*, 2078–2079. https://doi.org/10.1093/bioinformatics/btp352.
96. Pedersen, B.S., and Quinlan, A.R. (2018). Mosdepth: quick coverage calculation for genomes and exomes. Bioinformatics *34*, 867–868. https://doi.org/10.1093/bioinformatics/btx699.
97. Wickham, H. (2016). ggplot2: elegant graphics for data analysis (Springer-Verlag).
98. Breuer, M.R., Dasgupta, A., Vasselli, J.G., Lin, X., Shaw, B.D., and Sachs, M.S. (2022). The antidepressant sertraline induces the formation of supersized lipid droplets in the human pathogen Cryptococcus neoformans. J. Fungi *8*, 642. https://doi.org/10.3390/jof8060642.
99. Kim, D., Paggi, J.M., Park, C., Bennett, C., and Salzberg, S. L. (2019). Graph-based genome alignment and genotyping with HISAT2 and HISAT-genotype. Nat. Biotechnol. *37*, 907-915. https://doi.org/10.1038/s41587-019-0201-4.

100. Liao, Y., Smyth, G.K., and Shi, W. (2014). featureCounts: an efficient general purpose program for assigning sequence reads to genomic features. Bioinformatics *30*, 923–930. https://doi.org/10.1093/bioinformatics/btt656.
101. Love, M.I., Huber, W., and Anders, S. (2014). Moderated estimation of fold change and dispersion for RNA-seq data with DESeq2. Genome Biol. *15*, 550. https://doi.org/10.1186/s13059-014-0550-8.
102. Kerkaert, J.D., Le Mauff, F., Wucher, B.R., Beattie, S.R., Vesely, E.M., Sheppard, D.C., Nadell, C.D., and Cramer, R.A. (2022). An alanine aminotransferase is required for biofilm-specific resistance of Aspergillus fumigatus to echinocandin treatment. mBio *13*, e02933-21. https://doi.org/10.1128/mbio.02933-21.
103. Zhao, C., Fraczek, M.G., Dineen, L., Lebedinec, R., Macheleidt, J., Heinekamp, T., Delneri, D., Bowyer, P., Brakhage, A.A., and Bromley, M. (2019). High-throughput gene replacement in Aspergillus fumigatus. Curr. Protoc. Microbiol. *54*, e88. https://doi.org/10.1002/cpmc.88.
104. Beattie, S.R., Mark, K.M.K., Thammahong, A., Ries, L.N.A., Dhingra, S., Caffrey-Carr, A.K., Cheng, C., Black, C.C., Bowyer, P., Bromley, M.J., et al. (2017). Filamentous fungal carbon catabolite repression supports metabolic plasticity and stress responses essential for disease progression. PLOS Pathog. *13*, e1006340. https://doi.org/10.1371/journal.ppat.1006340.
105. Livak, K.J., and Schmittgen, T.D. (2001). Analysis of relative gene expression data using real-time quantitative PCR and the 2−ΔΔCT method. Methods *25*, 402–408. https://doi.org/10.1006/meth.2001.1262.
106. Adusumilli, R., and Mallick, P. (2017). Data conversion with ProteoWizard msConvert. Methods Mol. Biol. *1550*, 339–368. https://doi.org/10.1007/978-1-4939-6747-6_23.
107. Schmid, R., Heuckeroth, S., Korf, A., Smirnov, A., Myers, O., Dyrlund, T.S., Bushuiev, R., Murray, K.J., Hoffmann, N., Lu, M., et al. (2023). Integrative analysis of multimodal mass spectrometry data in MZmine 3. Nat. Biotechnol. *41*, 447–449. https://doi.org/10.1038/s41587-023-01690-2.
108. Nothias, L.-F., Petras, D., Schmid, R., Dührkop, K., Rainer, J., Sarvepalli, A., Protsyuk, I., Ernst, M., Tsugawa, H., Fleischauer, M., et al. (2020). Feature-based molecular networking in the GNPS analysis environment. Nat. Methods *17*, 905–908. https://doi.org/10.1038/s41592-020-0933-6.
109. Shannon, P., Markiel, A., Ozier, O., Baliga, N.S., Wang, J.T., Ramage, D., Amin, N., Schwikowski, B., and Ideker, T. (2003). Cytoscape: a software environment for integrated models of biomolecular interaction networks. Genome Res. *13*, 2498–2504. https://doi.org/10.1101/gr.1239303.
110. Ory, L., Gentil, E., Kumla, D., Kijjoa, A., Nazih, E.-H., and Roullier, C. (2020). Detection of ergosterol using liquid chromatography/electrospray ionization mass spectrometry:

investigation of unusual in-source reactions. Rapid Commun. Mass Spectrom. *34*, e8780. https://doi.org/10.1002/rcm.8780.

111. Chung, D., Barker, B.M., Carey, C.C., Merriman, B., Werner, E.R., Lechner, B.E., Dhingra, S., Cheng, C., Xu, W., Blosser, S.J., et al. (2014). ChIP-seq and in vivo transcriptome analyses of the Aspergillus fumigatus SREBP SrbA reveals a new regulator of the fungal hypoxia response and virulence. PLOS Pathog. *10*, e1004487. https://doi.org/10.1371/journal.ppat.1004487.

112. Rex, J. H., Alexander, B. D., Andes, D., Arthington-Skaggs, B., Brown, S. D., Chaturveli, V., Espinel-Ingroff, A., Ghannoum, M. A., Knapp, C. C., Motyl, M. R., Ostrosky-Zeicher, L., et al. (2008). Reference method for broth dilution antifungal susceptibility testing of filamentous fungi, approved standard. Second edition. M38-A2. Clin. Lab. Stand. Inst. *28*, 1–35.